

Physical Mechanisms Shaping the *Drosophila* Dorsoventral Compartment Boundary

Maryam Aliee,^{1,4} Jens-Christian Röper,^{2,3,4}
Katharina P. Landsberg,² Constanze Pentzold,^{2,5}
Thomas J. Widmann,^{2,6} Frank Jülicher,^{1,*}
and Christian Dahmann^{2,3,*}

¹Max Planck Institute for the Physics of Complex Systems,
Nöthnitzer Strasse 38, 01187 Dresden, Germany

²Max Planck Institute of Molecular Cell Biology and Genetics,
Pfotenhauerstrasse 108, 01307 Dresden, Germany

³Institute of Genetics, Dresden University of Technology,
01062 Dresden, Germany

Summary

Background: Separating cells with distinct identities and fates by straight and sharp compartment boundaries is important for growth and pattern formation during animal development. The physical mechanisms shaping compartment boundaries, however, are not fully understood.

Results: We combine theory and quantitative experiments to investigate the roles of different mechanisms to shape compartment boundaries. Our theoretical work shows that cell elongation created by anisotropic stress, cell proliferation rate, orientation of cell division, and cell bond tension all have distinct effects on the morphology of compartment boundaries during tissue growth. Our experiments using the developing *Drosophila* wing reveal that the roughness of the dorsoventral compartment boundary is dynamic and that it decreases during development. By measuring tissue relaxation in response to laser ablation of cell bonds at different developmental times, we demonstrate that decreased boundary roughness correlates with increased cell bond tension along the compartment boundary. Finally, by using experimentally determined values for cell bond tension, cell elongation and bias in orientation of cell division in simulations of tissue growth, we can reproduce the main features of the time evolution of the dorsoventral compartment boundary shape.

Conclusions: Local increase of cell bond tension along the boundary as well as global anisotropies in the tissue contribute to shaping boundaries in cell networks. We propose a simple scenario that combines time-dependent cell bond tension at the boundary, oriented cell division, and cell elongation in the tissue that can account for the main features of the dynamics of the shape of the dorsoventral compartment boundary.

Introduction

During animal development, cells collectively organize to form complex patterns and morphologies. Many proliferating

tissues are organized into cellular compartments separated by boundaries of cell lineage that play important roles as organizers in patterning processes [1–9]. These compartment boundaries prevent the mixing of adjacent cell populations and are characterized by a straight and smooth morphology.

The developing *Drosophila* wing (wing disc) is an excellent model system to study the mechanisms that shape compartment boundaries. The wing disc is a single-layered epithelium [10], which is set aside in the embryo as a group of approximately 50 cells subdivided into anterior and posterior compartments [11]. It grows during larval development in approximately 10 rounds of cell division to about 50,000 cells. A second compartment boundary, subdividing the wing disc into dorsal and ventral compartments (D/V boundary), arises during midlarval (60 hr after egg lay [AEL]; midsecond instar) development [11–13]. Maintenance of both compartment boundaries requires the activity of selector genes and signaling pathways [14–21].

We have previously shown that at the *Drosophila* anteroposterior compartment boundary, cell bond tension is increased as compared to the tissue [22] (see also [23]). This cell bond tension is generated along the adherens junctions linking two cells by the combination of actomyosin contractility and cell-cell adhesion. Local increases in cell bond tension are sufficient to prevent mixing of cells during cell proliferation and control the shape of boundaries [22]. It has been suggested that this locally increased cell bond tension results from signaling across the boundary [22, 24].

At the D/V boundary, nonmuscle myosin II (myosin II) and F-actin are enriched during midlarval development [25, 26], which has been interpreted as signs of increased tension [25, 26]. Furthermore, cells in the vicinity of the D/V boundary divide with their division plane frequently perpendicular to this boundary [25, 27]. It has been proposed that such an oriented cell division might influence boundary shape [25, 28]. Moreover, at late larval development, cell proliferation rate is reduced in an approximately 10–20 μm wide strip of cells centered on the D/V boundary [29], which has led to the proposal that this might be important for boundary shape [23, 25, 29, 30]. Finally, cells are typically elongated along the D/V boundary (see below), raising the question whether tissue anisotropies contribute to shaping compartment boundaries.

Here we use a combination of theory and quantitative experiments to study the role of different physical mechanisms for shaping compartment boundaries. We propose a simple scenario combining time-dependent cell bond tension, cell elongation, and oriented cell division that can quantitatively account for the main features of the dynamics of the D/V boundary morphology.

Results

Theoretical Analysis of Physical Mechanisms Shaping Compartment Boundaries

The shape of compartment boundaries in epithelial tissues is particularly well defined at the level of adherens junctions [22, 25], indicating that mechanisms, which maintain them, act at this cellular level. To identify and analyze physical

⁴These authors contributed equally to this work

⁵Present address: Department of Biology, University of Copenhagen, Ole Maaløes Vej 5, 2200 Copenhagen N, Denmark

⁶Present address: Centre for Genomics and Oncological Research, University of Granada, Avda. de la Ilustración 114, 18007 Granada, Spain

*Correspondence: julicher@pks.mpg.de (F.J.), christian.dahmann@mailbox.tu-dresden.de (C.D.)

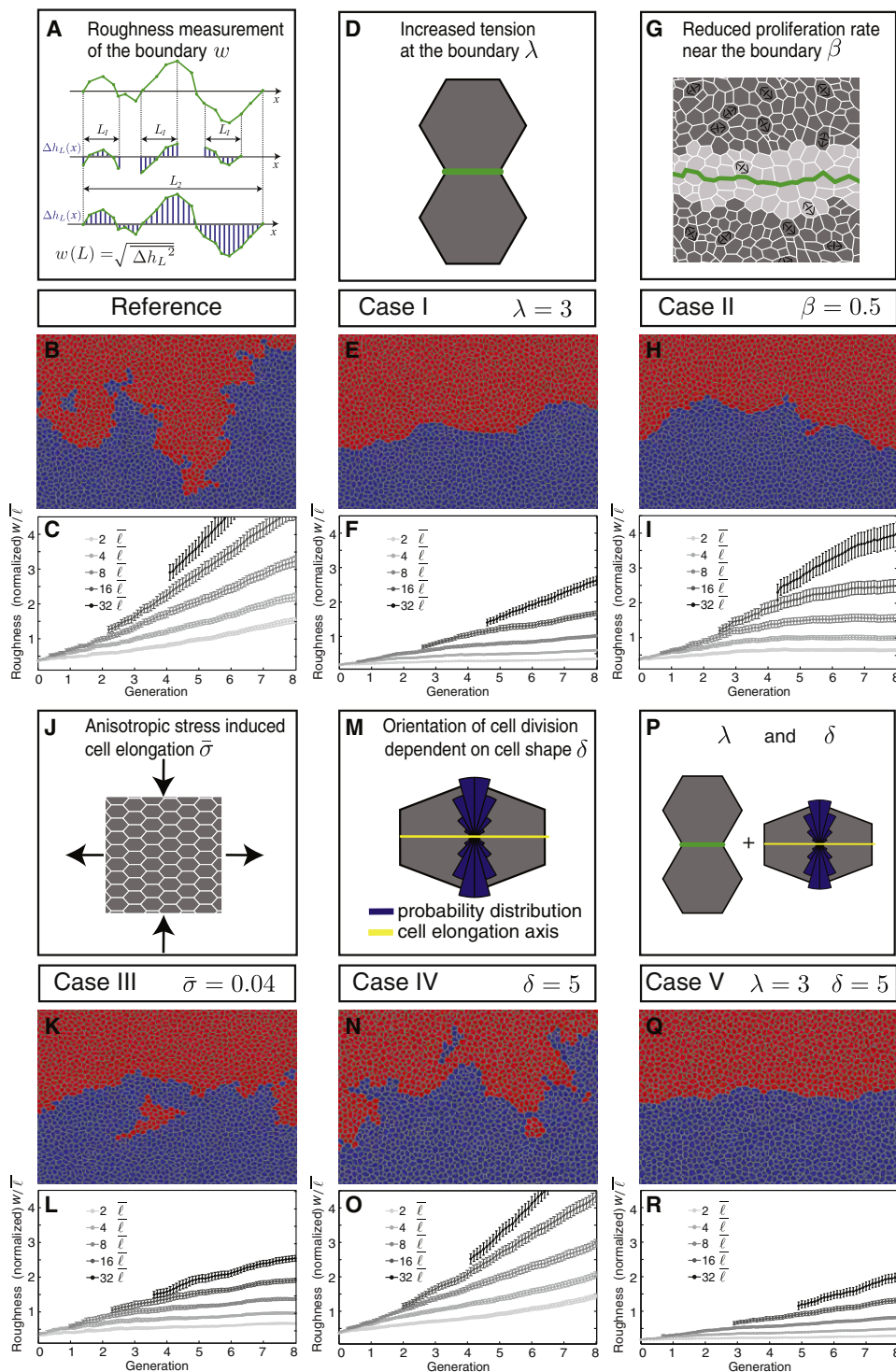


Figure 1. Time Evolution of the Morphology of the Boundary between Two Adjacent Cell Populations during Simulated Tissue Growth

(A) For any distance L along the boundary (x axis) $\Delta h_L(x)$ describes the shape of the boundary (green line) relative to the average line within the distance L . The roughness of the boundary $w(L)$ for the distance L is quantified by averaging $(\Delta h_L(x))^2$ within the distance L and along the boundary (see Supplemental Experimental Procedures).

(B–R) First and fourth rows illustrate the physical mechanisms. Green lines depict boundaries. Second and fifth rows represent examples of final configurations of networks of cell bonds of two adjacent cell populations (red and blue) at generation $G = 8$. Third and sixth rows depict roughness w of the boundary as function of generation G for indicated distances L along boundary given as multiples of average cell bond length $\bar{\ell}$. Distance and roughness values are normalized by $\bar{\ell}$. Mean and SEM are shown ($n = 10$ simulations).

(B and C) Reference case: all cells and cell bonds have same properties.

(D–F) Case I: cell bond tension is increased along boundary by factor $\lambda = 3$.

(G–I) Case II: rate of cell division is reduced by factor $\beta = 0.5$ in two rows of cells on both sides of boundary.

mechanisms that shape compartment boundaries and prevent mixing of cells from different compartments in proliferating epithelia, we simulated tissue growth using a vertex model [22, 31]. The vertex model describes the adherens junctional network by polygons. Stable force balance configurations of this network depend on physical parameters that characterize the mechanical properties of cells and cell bond tension. We introduced compartments in this model by starting from configurations of two adjacent cell populations separated by a well-defined boundary. Growth was simulated by stochastic cell divisions each of which involved the doubling of cell area and the addition of a new cell bond through the center of the cell. The junctional network was then remodeled to satisfy local force balance conditions. As a result, the shape of the boundary between two compartments changed over time. We characterized the boundary morphology by a geometric measure termed “roughness,” which characterizes the average distance of excursions of the boundary away from a straight line as a function of the length traveled along this line (Figure 1A) [22]. This roughness measure is therefore given as a function of the length along the boundary [32] (see [Supplemental Experimental Procedures](#) available online). In a tissue growing due to stochastic cell divisions, roughness typically increases as a function of length along the boundary because for larger lengths, the average excursions away from a straight line are bigger. We first considered a reference case, where cell division orientation is random and where cell bond tension along the compartment boundary is the same as for other bonds. In this case, the roughness of the compartment boundary measured over a fixed distance increased as a function of time (generation number) (Figures 1B and 1C; Figures S1A, S1A', and S1W; [Movie S1](#)), consistent with the notion that cell rearrangements caused by cell divisions induce boundary irregularities, which accumulate with time. In addition, cells of both populations started to mix (Figure 1B). We then investigated the influence of five different physical mechanisms that affect rearrangements of junctions during tissue growth and thus could play a role in shaping boundaries. We first analyzed local increases in cell bond tension along the compartment boundary by a factor λ as compared to the remaining tissue (Figure 1D, case I). Choosing $\lambda = 2, 3,$ or 4 resulted in a significant reduction of compartment boundary roughness compared to the reference case, and cells did not mix (Figures 1E–1F; Figures S1B–S1D'; [Movie S1](#)). Reducing the proliferation rate of cells close to the compartment boundary to 30% or 50% (described by the parameter β) (Figure 1G, case II) led to a similar decrease in roughness compared to case I, and cells also did not mix (Figures 1H and 1I; Figures S1E–S1G'). In case III, we simulated cell elongation parallel to the compartment boundary by applying dimensionless external shear stress (parameter $\bar{\sigma}$) to the cell network (Figure 1J, see [Supplemental Experimental Procedures](#)). This reduced boundary roughness but did not prevent cell mixing (Figures 1K and 1L; Figures S1H–S1J'). In case IV, we took into account that cells preferentially divide perpendicular to their long axis (e.g., [33]). The strength of this alignment is described by the parameter δ (Figure 1M, [Supplemental Experimental Procedures](#)). In the simulations, this alone had

no influence on boundary roughness and cell mixing (Figures 1N and 1O; Figures S1K–S1L', compare to reference case). However, when this preferential cell division orientation was introduced in conjunction with local increases in cell bond tension (Figure 1P, case V), then boundary roughness was further reduced (Figures 1Q and 1R; Figures S1M–S1O', compare to case I). Local increases in cell bond tension influence the orientation of cell elongation near the compartment boundary (Figures S1P–S1Q'). The elongation pattern that arises on average at curved boundaries contributes to a reduction of boundary roughness by influencing the average orientation of cell divisions (see [Supplemental Experimental Procedures](#); Figures S1P–S1Q'). Finally, we tested the effects of the dependence of the cell division probability on cell area pressure, which is the stress associated with cell area changes (Figure S1R; see [Supplemental Experimental Procedures](#)). This mechanism had, however, even in combination with local increases in cell bond tension, no considerable effect on boundary morphology (Figures S1S–S1V, cases VI and VII). We conclude that increased cell bond tension, reduced cell proliferation, and external shear stress can influence the morphology of compartment boundaries and have distinct effects. Oriented cell division influences boundary morphology only when local cell bond tension is increased.

Measurement of Boundary Roughness and Estimation of Stress Anisotropy and Bias of Cell Division Orientation

We next quantified the roughness of the D/V boundary and the morphology of wing disc cells in the vicinity of this boundary at different developmental times (Figures S2A–S2G) and calculated external shear stress $\bar{\sigma}$ and the strength of the bias in cell division orientation δ . Wing discs were stained for E-cadherin, a marker for adherens junctions, and a membrane-associated GFP, CD8-GFP, was expressed in dorsal cells under control of the *ap-GAL4* line [34] (Figures 2A–2E'). Automated image analysis was used to determine cell area, cell shape, and the roughness of the D/V boundary (Figures 2F–2J). Notably, the roughness started with comparably high values at 72 hr and 84 hr AEL but was then reduced at 96 hr, 108 hr, and 120 hr AEL (Figures 2F–2L). Interestingly, cells in the vicinity of the D/V boundary (10 cell rows dorsal and ventral) were elongated with a typical ratio of long to short axis of 1.1–1.3 parallel to the D/V boundary at all time points analyzed (Figure 2M). We estimated the value $\bar{\sigma} \sim 0.05$ of dimensionless shear stress by matching cell elongation in our simulations to those observed in the wing disc near the D/V boundary (Figure 2N; see [Supplemental Experimental Procedures](#)). We estimated the parameter δ describing the influence of cell elongation on cell division orientation as $\delta \sim 5$ based on observed cell division angle distributions [33] (Figure 2O; see [Supplemental Experimental Procedures](#)).

Local Reduction in Cell Proliferation Rate Is Not Required to Maintain the D/V Boundary

We next determined the relative rate of cell proliferation between cells in the vicinity of the D/V boundary and cells elsewhere in the wing disc for different developmental times. Cells replicating DNA were labeled by bromodeoxyuridine

(J–L) Case III: anisotropic stress of relative strength $\bar{\sigma} = 0.04$ is applied to stretch network parallel to boundary.

(M–O) Case IV: orientation of cell division is biased by coefficient $\delta = 5$.

(P–R) Case V: cell bond tension is increased along boundary by factor $\lambda = 3$ and orientation of cell division is biased by coefficient $\delta = 5$.

See also [Figure S1](#).

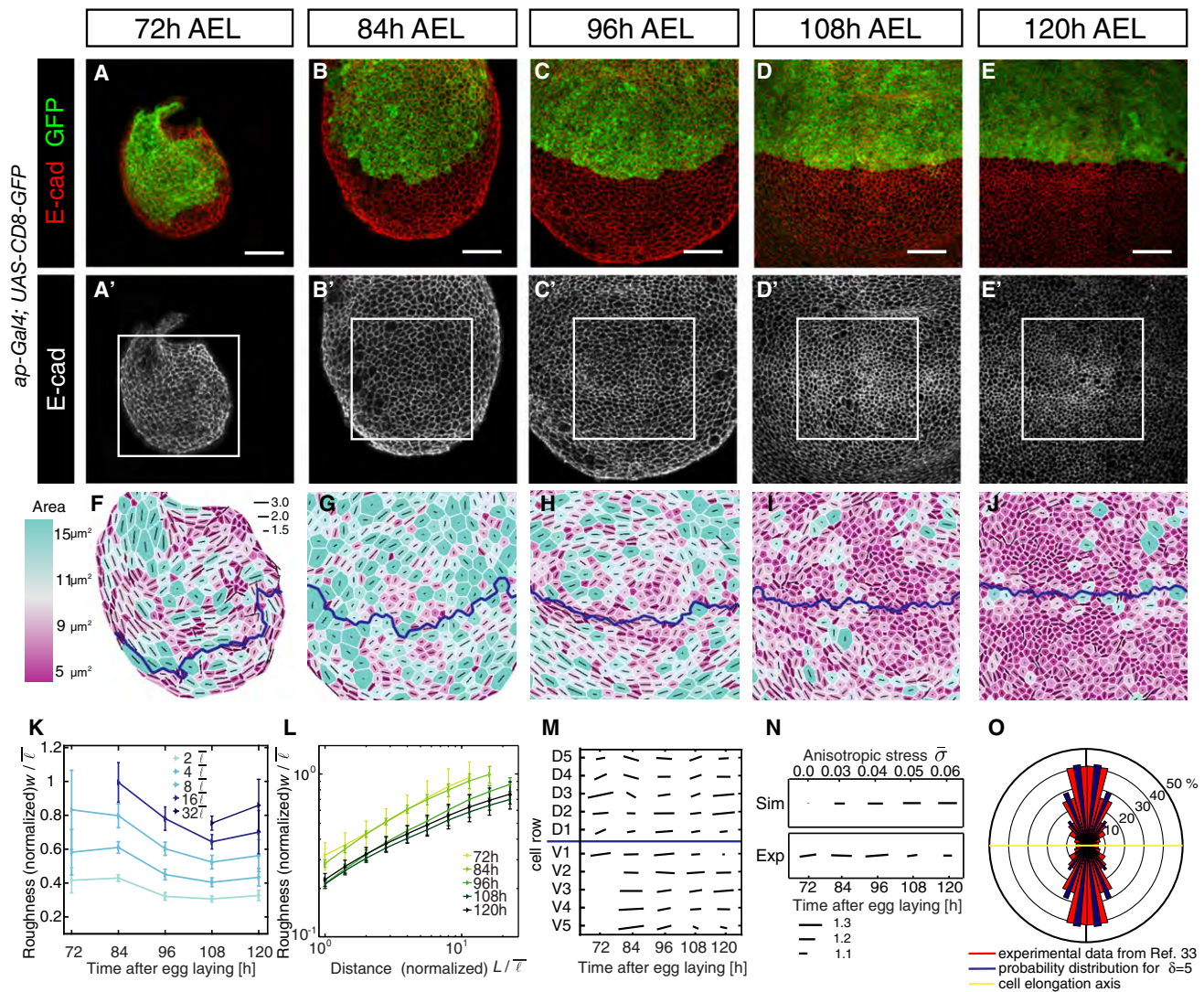


Figure 2. Measurement of the Roughness of the D/V Boundary and Estimates of Relative Strength of Stress Anisotropy and Bias in Orientation of Cell Division Axis

(A–E) Wing discs of indicated times AEL stained for E-cadherin (red). Dorsal compartments express CD8-GFP (green).

(F–J) Segmentations of areas boxed in (A')–(E'). Apical cross sectional area is color coded (left). Blue lines demarcate D/V boundary. Lengths of black bars represent ratio of long to short axis of a cell (see Supplemental Experimental Procedures).

(K) Roughness w of boundary as function of time AEL for indicated distances L shown as multiples of average cell bond length \bar{l} . Mean and SEM are shown. Roughness w is normalized to \bar{l} of each analyzed wing disc. Average cell bond length \bar{l} varies over time as cell area decreases, yet our conclusions do not depend on this choice of normalization (Figures S2H–S2J).

(L) Roughness w of boundary as function of distance L normalized to average cell bond length \bar{l} for indicated times AEL. Values are normalized as in (K). Mean and SEM are shown. Comparing 84 hr and 96 hr AEL, $p = 0.005–0.04$ for different L ; student's t test.

(M) Average cell elongation of cell rows along D/V boundary (D1, D2) and consecutive cell rows further away (D2, ..D5; V2, ..V5) of analyzed region for indicated time points. Blue line demarcates D/V boundary. Length of bars represents ratio of long to short axis of a cell parallel to D/V boundary (see N).

(N) Comparison of average cell elongation between simulation (Sim) for indicated values of $\bar{\sigma}$ and wing disc at indicated times AEL (Exp). Length of bars is as described in (M).

(O) Comparison between probability distribution of cleavage plane orientation from cell elongation axis in wing disc [33] and function for the probability of division orientation using vertex model for $\delta = 5$. Yellow line shows axis of cell elongation used as reference angle for each cell. Bars show the probability (expressed as radial distance from the center) of cells to divide with a given angular deviation from the long cell axis, averaged within 15° angle intervals. Angles range from 0° to 90° and are shown in the three other quadrants symmetrically.

For (K)–(N), $n = 5$ (72 hr), 6 (84 hr), 8 (96 hr), 9 (108 hr), and 7 (120 hr) wing discs.

Scale bars represent $20 \mu\text{m}$. See also Figure S2.

(BrdU) incorporation and the ratio of labeled to unlabeled cells was determined. At 84 hr and 96 hr AEL, the rate of cell proliferation was uniform throughout the wing disc (Figures S3A, S3B, S3F, and S3G) [35]. At later time points, cell proliferation rate was reduced ~ 1.5 fold in a strip of 5–10 cells (108 hr AEL;

Figures S3C and S3H [29]), or ~ 2.5 -fold within a strip of 10–20 cells (120 hr AEL; Figures 3A and 3C; Figures S3D, S3E, and S3I [29, 35]), centering on the D/V boundary.

To test whether this local decrease in cell proliferation rate is important for the morphology of the D/V boundary, we

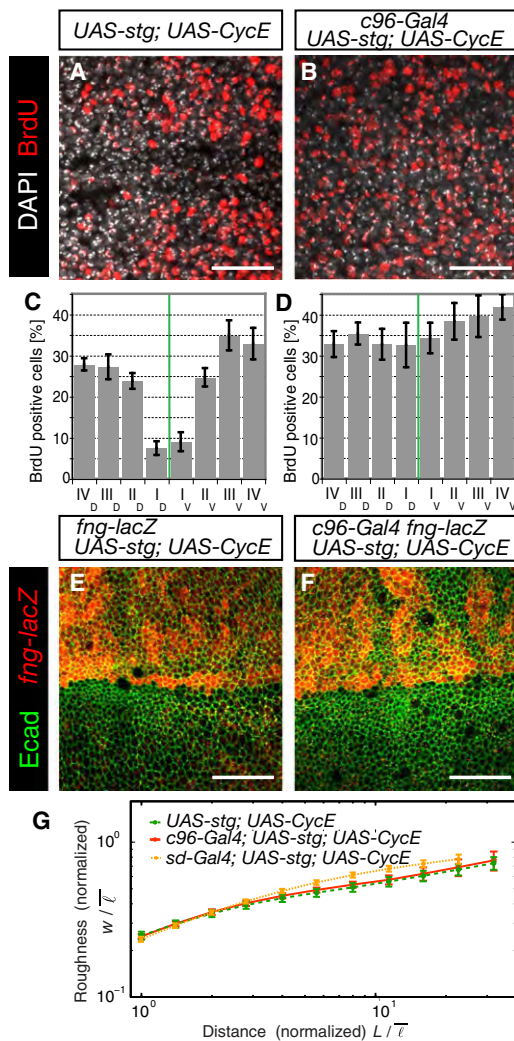


Figure 3. Local Reduction in the Rate of Cell Proliferation Is Not Required to Maintain a Straight and Sharp D/V Boundary

(A and B) Control wing disc (A) and wing disc coexpressing *string* and *cyclin E* in the vicinity of the D/V boundary (B) at 120 hr AEL stained for BrdU (red) and DAPI (white). Position of D/V boundary is inferred from the more basal position of nuclei in cells at D/V boundary compared to position of nuclei in neighboring cells.

(C and D) Percentage of BrdU-positive cells of control wing discs (C) and wing discs coexpressing *string* and *cyclin E* in vicinity of D/V boundary (D) at 120 hr AEL. I_D to IV_D and I_V to IV_V refer to consecutive 10 μm broad strips of cells at D/V boundary (I_D and I_V) and further away in dorsal and ventral compartments, respectively. Mean and SEM are shown (n = 6 [control], n = 6 [coexpressing *string* and *cyclin E*] wing discs).

(E and F) Control wing disc (E) and wing disc coexpressing *string* and *cyclin E* in vicinity of D/V boundary under control of *c96-Gal4* (F) at 120 hr AEL stained for E-cadherin (green) and *fng-lacZ* (35UZ-1; red), a marker for the dorsal compartment [45].

(G) Roughness w of D/V boundary as function of distance L parallel to boundary normalized by average bond length \bar{l} for genotypes shown as indicated. Mean and SEM are shown: $p = 0.6$ – 0.9 for different L , $n = 6$. Scale bars represent (A and B) 20 μm and (E and F) 10 μm. See also Figure S3.

increased the rate of cell proliferation by coexpressing the cell-cycle regulators *string* and *cyclin E* in the wing disc using the *c96-GAL4* [36] or *sd-Gal4* [37] lines. As a consequence, cell proliferation rate in the vicinity of the D/V boundary was indistinguishable from the cell proliferation rate elsewhere in the

tissue at 108 hr AEL (Figures S3J–S3M) and 120 hr AEL (Figures 3B and 3D) [38]. The roughness of the D/V boundary was indistinguishable between control wing discs and discs coexpressing *string* and *cyclin E* (Figures 3E–3G; Figures S3N–S3R). These data differ from a recent report suggesting that stimulation of cell proliferation along the D/V boundary results in rougher boundaries [30]. Although we do not understand the cause of this discrepancy, we note that in Becam et al. [30] D/V boundary shape was measured at the level of nuclei, whereas we determined boundary roughness at the level of adherens junctions, where the D/V boundary is most well-defined. We conclude from our data that a decreased cell proliferation rate during late larval development is not important to maintain a straight and sharp D/V boundary.

A Local Increase in Mechanical Tension along the D/V Boundary

We next estimated the mechanical tension on cell bonds along the D/V boundary relative to tension along other cell bonds in wing discs. Tissue relaxation in response to ablating single cell bonds provides a direct and quantitative indicator of mechanical tension on cell bonds [39]. We ablated individual cell bonds using an UV-laser beam at different developmental times and analyzed the resulting displacement of cell vertices (Figure 4A) [22]. Cell bonds were identified using E-cadherin-GFP and the dorsal compartment was identified by expression of a *gpi*-linked GFP (GFP-*gpi*) [40] under control of *ap-GAL4*. The maximal increase of distance between vertices upon cell bond ablation within the dorsal or ventral compartments was similar to each other for all time points (Figures 4B–4G; Movie S2). This was also the case when we specifically ablated cell bonds between the first and second row of dorsal cells (D1/D2) or between the first and second row of ventral cells (V1/V2) (Figure 4G; Figures S4A and S4B). The maximal vertex distance increase was also similar when cell bonds along the borders of the expression domain of the transcription factor *Cut* were ablated (Figures S4C and S4O). *Cut* defines a boundary cell population important for maintaining the D/V boundary during late larval development [30]. At 84 hr AEL, the vertex distance increase after ablating cell bonds along the D/V boundary was slightly larger compared to ablation in the dorsal and ventral compartments (Figures 4C and 4G). For 96 hr, 108 hr, and 120 hr AEL, the vertex distance increase was significantly larger for D/V bonds (Figures 4B and 4D–4G; Movie S2). Vertex distance increases of ablated D/D and D/V bonds were reduced in the presence of the Rho-kinase inhibitor Y-27632 [41] (Figure 4G; Figures S4D and S4E), whose main target is myosin II [42], indicating that cell bond tension in the wing disc depends on myosin II activity [22, 31]. Interestingly, even though reduced, the vertex distance increase was still higher for ablated D/V bonds than for D/D bonds (Figure 4G; Figures S4D and S4E), suggesting that the relative difference in cell bond tension may be regulated, in part, independently of myosin II activity. Taken together, these results demonstrate that cell bond tension is locally increased along the D/V boundary during mid-to-late third-instar larval development.

We estimated the ratio between cell bond tension along the D/V boundary and average cell bond tension in the tissue, λ , by comparing the experimental data to simulations of laser ablations in our vertex model. The most robust estimate was obtained by comparing radial displacements of vertices in the vicinity of the ablation between experiment and simulations. We first quantified the experimentally observed radial

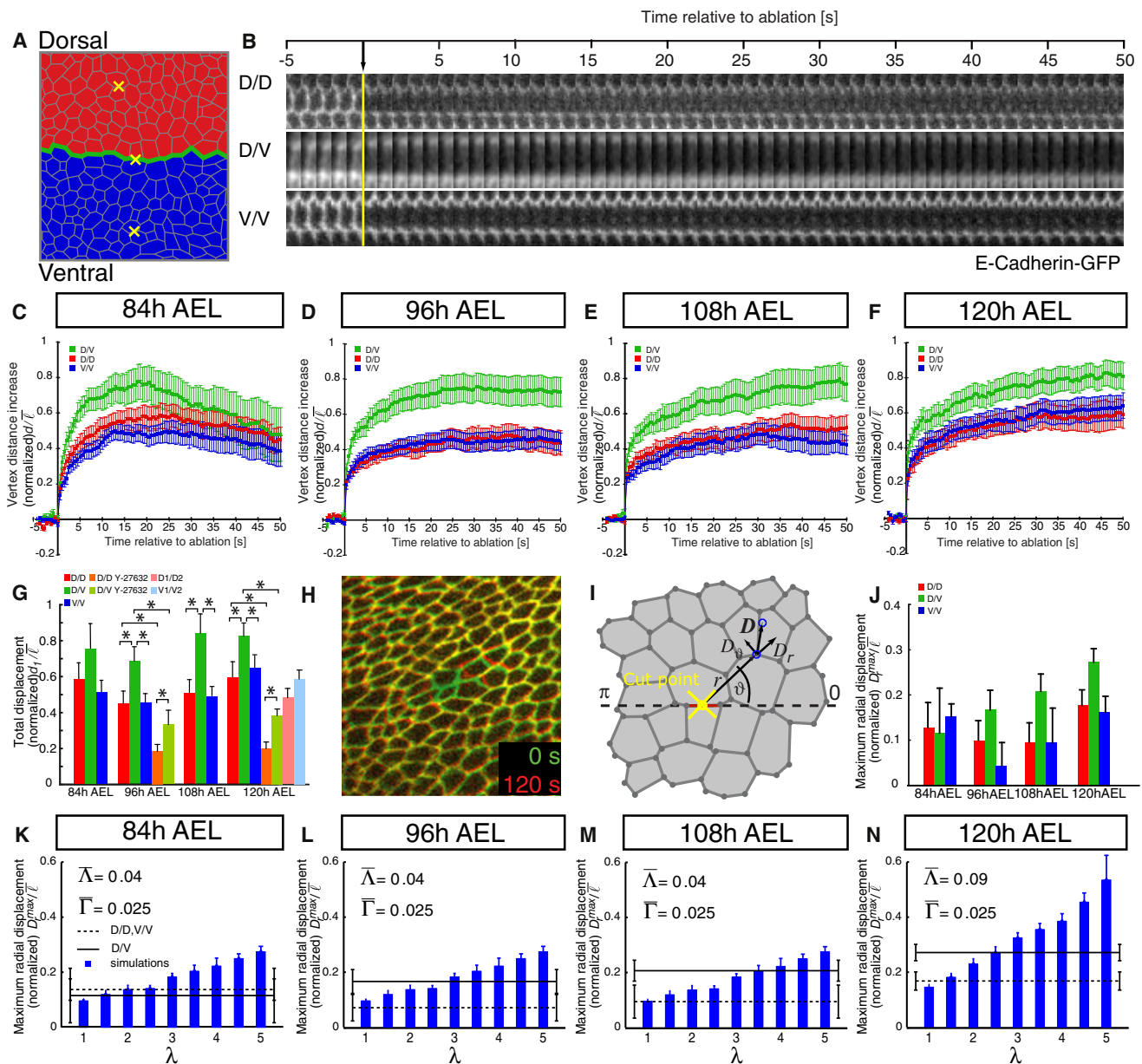


Figure 4. Laser Ablation Reveals a Local Increase in Mechanical Tension on Cell Bonds along the D/V Boundary

(A) Scheme of network of adherens junctions. Dorsal and ventral cells are colored in red and blue, respectively. Green line indicates D/V boundary, and yellow crosses mark approximate location of laser ablations.

(B) Kymographs of D/D, D/V, and V/V cell bonds visualized by E-cadherin-GFP before and after laser ablation for wing discs at 96 hr AEL. Yellow line indicates time point of laser ablation. See also [Movie S2](#).

(C–F) Change in distance d between vertices at ends of cell bonds before and after ablation normalized to average bond length \bar{l} of each time point as function of time relative to ablation for wing discs 84 hr (C), 96 hr (D), 108 hr (E), and 120 hr (F) AEL. Types of ablated cell bonds are indicated. Mean and SEM are shown (84 hr: $n = 14$ ablations [D/D], 9 [D/V], 13 [V/V]; 96 hr: $n = 26$ [D/D], 22 [D/V], 18 [V/V]; 108 hr: $n = 17$ [D/D], 18 [D/V], 16 [V/V]; 120 hr: $n = 15$ [D/D], 19 [D/V], 15 [V/V]).

(G) Total displacement d_t of vertices at ends of ablated cell bonds for indicated types of cell bonds and developmental times. Values are normalized for average cell bond length \bar{l} of each time point. The mean and SEM of fits are shown (see [Supplemental Experimental Procedures](#)) (n as in C–F). Asterisks indicate $p < 0.05$; student's t test. See also [Figure S4](#).

(H) Overlay of images of wing discs expressing E-cadherin-GFP before (0 s, green) and 120 s after (red) laser ablation of single cell bond.

(I) Schematic representation of displacement vectors D with radial component D_r and tangential component D_θ of vertices located at distance r from the cut point (yellow cross), at angle ϑ relative to cut bond axis (dashed line).

(J) Maximum radial displacement D_r^{\max} determined by fits shown in [Figures S4F–S4I'](#) normalized to average bond length \bar{l} of each time point. Average values of D_r^{\max} and SE of fits are shown.

(K–N) Maxima of radial displacements D_r^{\max} for ablated D/V bonds (black line) and average D_r^{\max} of D/D and V/V bonds (dashed black line) for laser ablations at 84 hr (K) 96 hr (L), 108 hr (M), and 120 hr (N) AEL are shown. Maxima of radial displacements D_r^{\max} obtained from simulations of cell bond ablations with different λ are shown as blue bars.

Values of $\bar{\Lambda}$ and $\bar{\Gamma}$ used in simulations are indicated. Mean and SEM are shown ($n = 10$ simulations).

displacements of vertices as a function of angle relative to the orientation of ablated bonds (Figures 4H and 4I). Interestingly, the maximum radial displacements resulting from ablating cell bonds within the dorsal or ventral compartment were increased at 120 hr AEL compared to earlier time points (Figure 4J; Figures S4F–S4I’), indicating that the average cell bond tension in the tissue increases during late larval development. At 84 hr AEL, the maximal radial displacements resulting from ablating bonds along the D/V boundary and within the dorsal and ventral compartments were similar (Figure 4J; Figure S4F). For 96 hr, 108 hr, and 120 hr AEL, the maximal radial displacements of D/V bonds were increased as compared to the maximal radial displacements of D/D or V/V bonds (Figure 4J; Figures S4G–S4I’). We then simulated cell bond ablations in the vertex model for values of λ varying between 1 and 5. To account for the increased average cell bond tension at 120 hr, we used a larger value of tissue bond tension $\bar{\lambda}$ in the simulations of this time point. At 84 hr AEL, the maximum radial displacements in the experiment closely matched the radial displacement in the simulation when $\lambda = 1$ (Figure 4K). The maximum radial displacements in response to laser ablations at 96 hr, 108 hr, or 120 hr AEL corresponded to values of λ between 2.5 and 3.0 (Figures 4L–4N). These results demonstrate that cell bond tension along the D/V boundary varies over developmental time. At 84 hr AEL, cell bond tension along the D/V boundary is similar to cell bond tension in the tissue. By contrast, from 96 hr to 120 hr AEL, cell bond tension along the D/V boundary is approximately 2.5- to 3-fold increased.

We note that the increase in cell bond tension along the D/V boundary between 84 hr and 96 hr AEL coincides with the observed reduction of roughness (Figures 2K and 2L). This local increase in cell bond tension also coincides with elevated levels of myosin II and F-actin at this boundary (Figures S4J, S4K, and S4N) [25, 26]. During later larval development, however, cell bond tension along the D/V boundary is still increased, even though higher levels of F-actin and myosin II are no longer detected (Figures S4L–S4N) [25, 26], indicating that the amounts of F-actin and myosin II might not directly reflect the tension of cell bonds. Myosin II activity, however, plays an important role in shaping the D/V boundary, because the roughness of the D/V boundary was significantly increased in mutants for myosin heavy chain (encoded by *zipper*; *zip*^{2/zip^{ED1}) (Figures S4P–S4R) [26].}

Simulations of the Time Evolution of the D/V Boundary in the Vertex Model

We next tested whether the experimentally estimated values and time dependence of the analyzed parameters can account for the morphology of the D/V boundary during development. We simulated tissue growth during eight rounds of cell division, which approximately corresponds to the number of cell divisions that takes place in the wing disc between 48 hr and 120 hr AEL [43]. To resemble the establishment of the D/V boundary, we introduced a boundary separating two cell populations in the simulation after the third generation. Cell bond tension along this boundary was increased 3-fold between the fifth and sixth cell generation, similar to the situation in the wing disc (Figure 5A). This scenario (scenario I) resulted in a boundary that was significantly rougher than the D/V boundary observed in experiments (compare Figures 5B and 5C and Figures 2K and 2L; Figure S5A). We therefore in addition reduced the proliferation rate by 60% in five rows of cells on both sides of the boundary between generation seven and eight in the simulation (Figure 5D), similar to what is

observed in the wing disc. This scenario (scenario II) revealed that changes of cell proliferation rate near the D/V boundary at late stages of development have a weak effect on boundary morphology (Figures 5E and 5F, Figure S5B), consistent with our experimental findings (Figures 3E–3G). Scenario III was similar to scenario I, except that we took into account that cells are elongated parallel to the D/V boundary by subjecting the system to an externally applied anisotropic stress $\bar{\sigma} = 0.05$ starting from generation three (Figure 5G). Boundary roughness is significantly reduced as compared to scenarios I and II, but roughness is not decreasing as much as observed in experiments (Figures 5H–5I; Figure S5C). Finally, scenario IV combines a local increase in cell bond tension between generations five and six and an external anisotropic stress $\bar{\sigma} = 0.05$ after generation three with a bias in the orientation of cell division with $\delta = 5$ (Figure 5J). Most interestingly, with this scenario we can quantitatively account for the main features of the observed time evolution of roughness of the D/V boundary during development (Figures 5K–5N; Figure S5D; Movie S3). This includes the length dependence of roughness at early times and the reduction of roughness for different length at later times. In particular, this scenario can account for the decrease in roughness of the D/V boundary that is observed between 84 hr and 96 hr AEL (Figures 5M and 5N). We conclude that a combination of increased cell bond tension, cell elongation and/or stress, and oriented cell division are the key mechanisms to shape the D/V boundary.

Discussion

We have studied the role of tissue mechanics for the morphology of boundaries in growing cell networks using a vertex model. Previous work has demonstrated that local increases in cell bond tension can control boundary roughness [22]. Here we extended this work by studying the time evolution of boundary roughness during growth and we have identified three additional mechanisms that can significantly influence boundary roughness: orientation of cell division biased by cell elongation, reduced cell proliferation rate in cell rows next to the boundary, and overall cell elongation parallel to the boundary axis. In simulations of tissue growth, boundary roughness increases with time due to an accumulation of boundary shape fluctuations caused by stochastic cell divisions. Locally increased cell bond tension and reduced cell proliferation persistent over several generations reduce boundary roughness and prevent mixing of the two cell populations. Moreover, in conjunction with increased cell bond tension, a bias in orientation of cell division by cell elongation can significantly reduce boundary roughness. Interestingly, a significant reduction of roughness can also result from overall cell elongation in the tissue parallel to the boundary. Cell elongation could result from external stresses acting on the tissue or from anisotropies within the tissue. Such anisotropies could, for example, result from the activity of the planar cell polarity pathway [44]. Taken together, local effects at the boundary as well as global anisotropies within the whole tissue contribute to shaping boundaries in cell networks.

Mechanisms Governing the Morphology and Maintenance of the D/V Boundary

The roughness of the D/V boundary is initially high, but is then reduced during mid-third-instar larval development (Figure 6). Interestingly, this decrease in boundary roughness coincides with an increase in cell bond tension along the D/V boundary.

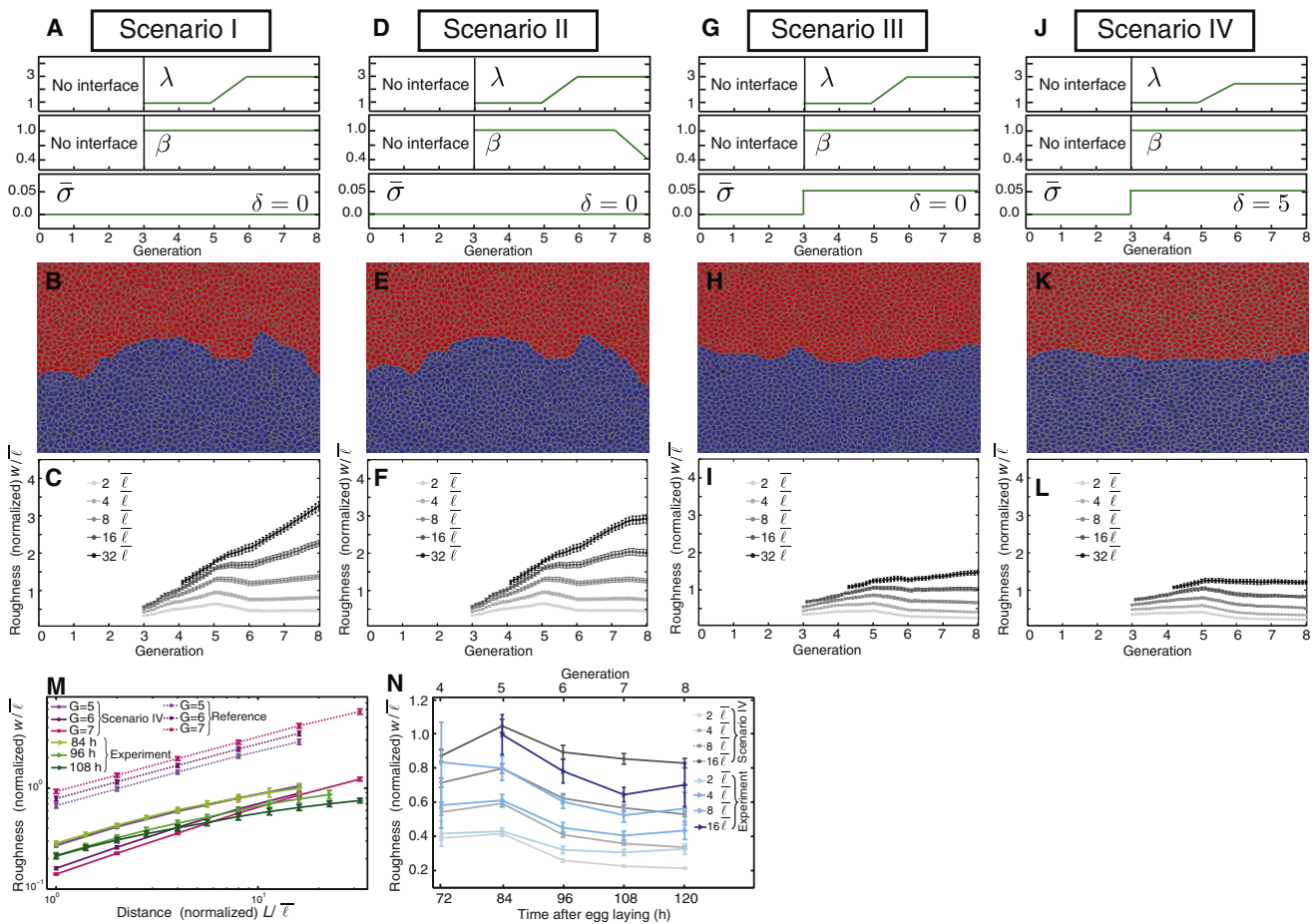


Figure 5. Growth Simulations Accounting for the Time Evolution of the Morphology of the D/V Boundary

(A–L) Straight boundary is introduced in the tissue at $G = 3$. All cells are identical until $G = 5$. Cell bond tension is increased along boundary between generations five and six, and it remains constant afterwards.

First line depicts parameter values used in simulations as function of generation number (see text). Second and third lines represent examples of final configurations and roughness w of boundaries as explained in legend to Figure 1. Mean and SEM are shown ($n = 10$ simulations).

(A–C) Scenario I: relative cell bond tension along boundary is increased by factor $\lambda = 3$ between generations five and six.

(D–F) Scenario II: as in scenario I, but rate of cell division is reduced during last generation by factor $\beta = 0.4$ in five rows of cells on both sides of boundary.

(G–I) Scenario III: as in scenario I, but anisotropic stress of relative strength $\bar{\sigma} = 0.05$ is applied to stretch network parallel to boundary after generation three.

(J–L) Scenario IV: orientation of cell division is biased by coefficient $\delta = 5$. Anisotropic stress of relative strength $\bar{\sigma} = 0.05$ is applied to stretch network parallel to boundary after generation three. Relative cell bond tension along boundary is increased by factor $\lambda = 2.5$ at generation six. See also [Movie S3](#).

(M and N) Comparison between roughness of D/V boundary (Experiment) at indicated times AEL and roughness of simulation boundaries in reference case and in scenario IV at different generations. Roughness is plotted as function of distance L along boundary (M) or times AEL (N).

We infer that, initially, D/V boundary morphology might be governed by stochasticity of cell division. The time period from establishing the D/V boundary to increasing cell bond tension encompasses approximately four rounds of cell division in wing discs. Our simulations indicate that four rounds of cell division only result in slight increases of boundary roughness in controls. Thus, mechanisms to maintain a sharp and straight D/V boundary might not be in effect during this time period. Once cell bond tension along the D/V boundary increases between 84 hr and 96 hr AEL as compared to the remaining tissue, it remains elevated for the rest of larval development. Increased cell bond tension governs cell rearrangements after cell division to reduce boundary roughness. Our simulations also indicate that increased cell bond tension leads locally to patterns of cell elongation in the vicinity of the D/V boundary (Figures S1P–S1Q) that lead to additional reduction of roughness if the cell division axis is biased by

cell elongation. Finally, the general elongation of cells parallel to the D/V boundary, which we observed during all developmental time points analyzed, could contribute to reduction in boundary roughness in particular for long boundary distances. Taken together, this simple scenario can account for the main features of the time evolution of the shape of the D/V boundary (Figures 5M and 5N).

In summary, our work demonstrates and quantifies an increase in cell bond tension along the D/V boundary from mid-to-late third-instar larval development in *Drosophila* wing discs. Moreover, we identify and characterize additional mechanisms that in general affect boundary morphology. Our work suggests that, at the D/V boundary, two of these mechanisms have a strong influence: oriented cell division and cell elongation. Both mechanisms, however, reduce boundary roughness and prevent cell mixing only in conjunction with a local increase of cell bond tension at the boundary. Thus,

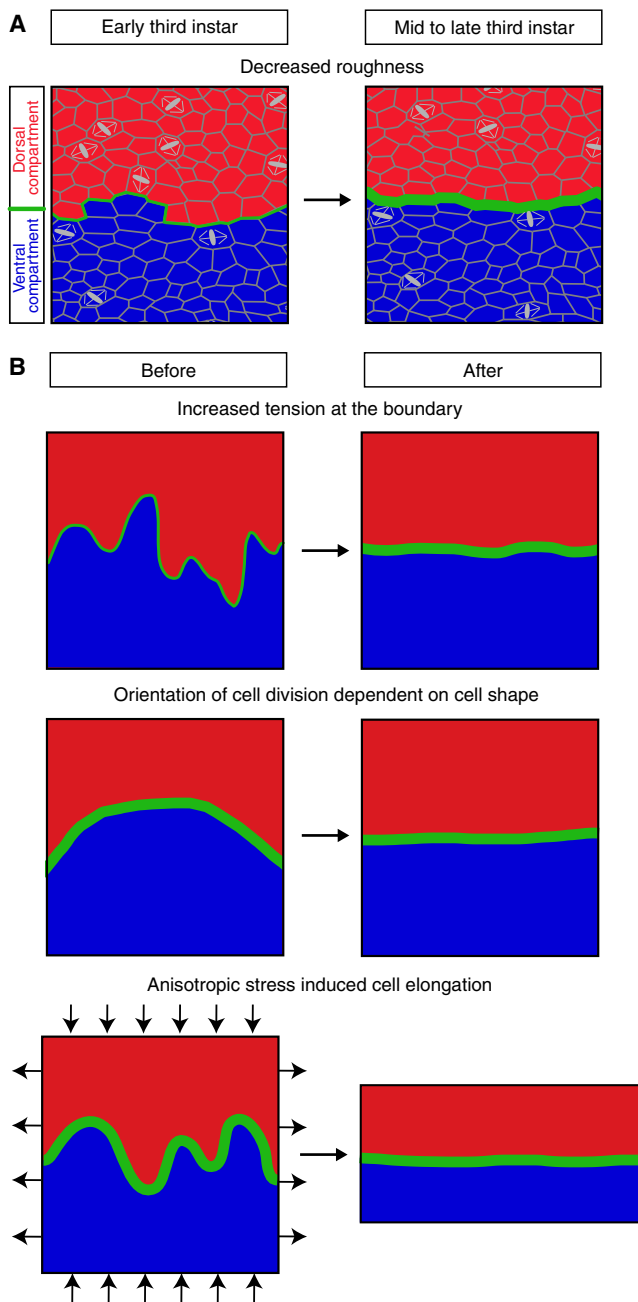


Figure 6. Mechanisms Shaping the D/V Boundary

(A) Description of networks of adherens junctions (gray) in dorsal (red) and ventral (blue) compartments of wing discs at indicated developmental times. In early third-instar larval development (left), roughness of D/V boundary is high, and cell bond tension at boundary (thin green line) is similar to elsewhere in the tissue. During mid-to-late third-instar larval development (right), roughness of D/V boundary is low and cell bond tension is increased along boundary (thick green line). During all of third-instar larval development, cells are preferentially elongated parallel to D/V boundary and orientation of division plane, indicated by a mitotic spindle, is biased by cell shape.

(B) Physical mechanisms shaping boundary between two compartments (red and blue). Local increase in cell bond tension (thin to thick green line) reduces boundary roughness and prevents mixing of two cell populations (top). In conjunction with a locally increased cell bond tension, a bias in cell division orientation by cell elongation further reduces boundary roughness (middle). Cell elongation and tissue shear caused by anisotropic tissue stress (arrows) contribute to reduced boundary roughness but only in conjunction with locally increased cell bond tension along boundary prevent mixing of the two cell populations (bottom).

a local increase in cell bond tension is the primary mechanism to maintain a straight and sharp D/V boundary. A challenge for the future will be the identification of the molecular mechanisms that locally increase mechanical tension along the D/V boundary. Our previous work has demonstrated an increase in mechanical tension confined to cell bonds along the antero-posterior compartment boundary in *Drosophila* wing discs [22]. Thus, a local increase in mechanical tension might be a common principal mechanism to maintain straight and sharp compartment boundaries in developing tissues.

Supplemental Information

Supplemental Information includes five figures, Supplemental Experimental Procedures, and three movies and can be found with this article online at doi:10.1016/j.cub.2012.03.070.

Acknowledgments

We are grateful to S. Grill and A.A. Hyman for providing us with the laser-ablation system. We thank I. Ibarlucea Benitez and S. Hennig for help with the laser ablation experiments; C. Ehrlich for help with developing software for image analysis; K. Basler, S. Eaton, K. Irvine, and the Bloomington *Drosophila* stock center for fly stocks; the Developmental Studies Hybridoma Bank for antibodies; and S. Grill, K. Neugebauer, and G. Salbreux for critical comments on the manuscript. This work was supported by the Max Planck Society and by grants from Deutsche Forschungsgemeinschaft (DA586/8-1 to C.D.) and the Human Frontier Science Program (RGP0052/2009 to C.D.).

Received: November 1, 2011

Revised: February 28, 2012

Accepted: March 27, 2012

Published online: May 3, 2012

References

- Blair, S.S. (2003). Developmental biology: boundary lines. *Nature* 424, 379–381.
- Dahmann, C., Oates, A.C., and Brand, M. (2011). Boundary formation and maintenance in tissue development. *Nat. Rev. Genet.* 12, 43–55.
- Irvine, K.D., and Rauskolb, C. (2001). Boundaries in development: formation and function. *Annu. Rev. Cell Dev. Biol.* 17, 189–214.
- Martin, A.C., and Wieschaus, E.F. (2010). Tensions divide. *Nat. Cell Biol.* 12, 5–7.
- McNeill, H. (2000). Sticking together and sorting things out: adhesion as a force in development. *Nat. Rev. Genet.* 1, 100–108.
- Monier, B., Pélissier-Monier, A., and Sanson, B. (2011). Establishment and maintenance of compartmental boundaries: role of contractile actomyosin barriers. *Cell. Mol. Life Sci.* 68, 1897–1910.
- Tepass, U., Godt, D., and Winklbauer, R. (2002). Cell sorting in animal development: signalling and adhesive mechanisms in the formation of tissue boundaries. *Curr. Opin. Genet. Dev.* 12, 572–582.
- Vincent, J.P. (1998). Compartment boundaries: where, why and how? *Int. J. Dev. Biol.* 42, 311–315.
- Vincent, J.P., and Irons, D. (2009). Developmental biology: tension at the border. *Curr. Biol.* 19, R1028–R1030.
- Cohen, S.M. (1993). Imaginal disc development. In *The Development of Drosophila melanogaster*, Volume 2, M. Bate and A. Martinez Arias, eds. (New York: Cold Spring Harbor Laboratory Press), pp. 747–841.
- Garcia-Bellido, A., Ripoll, P., and Morata, G. (1973). Developmental compartmentalization of the wing disk of *Drosophila*. *Nat. New Biol.* 245, 251–253.
- Bryant, P.J. (1970). Cell lineage relationships in the imaginal wing disc of *Drosophila melanogaster*. *Dev. Biol.* 22, 389–411.
- Garcia-Bellido, A., Ripoll, P., and Morata, G. (1976). Developmental compartmentalization in the dorsal mesothoracic disc of *Drosophila*. *Dev. Biol.* 48, 132–147.
- Blair, S.S., Brower, D.L., Thomas, J.B., and Zavortink, M. (1994). The role of *apterous* in the control of dorsoventral compartmentalization and PS integrin gene expression in the developing wing of *Drosophila*. *Development* 120, 1805–1815.

15. Blair, S.S., and Ralston, A. (1997). Smoothed-mediated Hedgehog signalling is required for the maintenance of the anterior-posterior lineage restriction in the developing wing of *Drosophila*. *Development* **124**, 4053–4063.
16. Dahmann, C., and Basler, K. (2000). Opposing transcriptional outputs of Hedgehog signaling and engrailed control compartmental cell sorting at the *Drosophila* A/P boundary. *Cell* **100**, 411–422.
17. Micchelli, C.A., and Blair, S.S. (1999). Dorsoventral lineage restriction in wing imaginal discs requires Notch. *Nature* **401**, 473–476.
18. Morata, G., and Lawrence, P.A. (1975). Control of compartment development by the *engrailed* gene in *Drosophila*. *Nature* **255**, 614–617.
19. Rauskolb, C., Correia, T., and Irvine, K.D. (1999). Fringe-dependent separation of dorsal and ventral cells in the *Drosophila* wing. *Nature* **401**, 476–480.
20. Rodriguez, I., and Basler, K. (1997). Control of compartmental affinity boundaries by hedgehog. *Nature* **389**, 614–618.
21. Shen, J., and Dahmann, C. (2005). The role of Dpp signaling in maintaining the *Drosophila* anteroposterior compartment boundary. *Dev. Biol.* **279**, 31–43.
22. Landsberg, K.P., Farhadifar, R., Ranft, J., Umetsu, D., Widmann, T.J., Bittig, T., Said, A., Jülicher, F., and Dahmann, C. (2009). Increased cell bond tension governs cell sorting at the *Drosophila* anteroposterior compartment boundary. *Curr. Biol.* **19**, 1950–1955.
23. Monier, B., Pélissier-Monier, A., Brand, A.H., and Sanson, B. (2010). An actomyosin-based barrier inhibits cell mixing at compartmental boundaries in *Drosophila* embryos. *Nat. Cell Biol.* **12**, 60–65, 1–9.
24. Schilling, S., Willecke, M., Aegerter-Wilmsen, T., Cirpka, O.A., Basler, K., and von Mering, C. (2011). Cell-sorting at the A/P boundary in the *Drosophila* wing primordium: a computational model to consolidate observed non-local effects of Hh signaling. *PLoS Comput. Biol.* **7**, e1002025.
25. Major, R.J., and Irvine, K.D. (2005). Influence of Notch on dorsoventral compartmentalization and actin organization in the *Drosophila* wing. *Development* **132**, 3823–3833.
26. Major, R.J., and Irvine, K.D. (2006). Localization and requirement for Myosin II at the dorsal-ventral compartment boundary of the *Drosophila* wing. *Dev. Dyn.* **235**, 3051–3058.
27. Baena-López, L.A., Baonza, A., and García-Bellido, A. (2005). The orientation of cell divisions determines the shape of *Drosophila* organs. *Curr. Biol.* **15**, 1640–1644.
28. Canela-Xandri, O., Sagués, F., Casademunt, J., and Buceta, J. (2011). Dynamics and mechanical stability of the developing dorsoventral organizer of the wing imaginal disc. *PLoS Comput. Biol.* **7**, e1002153.
29. O'Brochta, D.A., and Bryant, P.J. (1985). A zone of non-proliferating cells at a lineage restriction boundary in *Drosophila*. *Nature* **313**, 138–141.
30. Becam, I., Rafel, N., Hong, X., Cohen, S.M., and Milán, M. (2011). Notch-mediated repression of *bantam* miRNA contributes to boundary formation in the *Drosophila* wing. *Development* **138**, 3781–3789.
31. Farhadifar, R., Röper, J.C., Aigouy, B., Eaton, S., and Jülicher, F. (2007). The influence of cell mechanics, cell-cell interactions, and proliferation on epithelial packing. *Curr. Biol.* **17**, 2095–2104.
32. Barabasi, H.L., and Stanley, H.E. (1995). *Fractal Concepts in Surface Growth* (Cambridge: Cambridge University Press).
33. Gibson, W.T., Veldhuis, J.H., Rubinstein, B., Cartwright, H.N., Perrimon, N., Brodland, G.W., Nagpal, R., and Gibson, M.C. (2011). Control of the mitotic cleavage plane by local epithelial topology. *Cell* **144**, 427–438.
34. Calleja, M., Moreno, E., Pelaz, S., and Morata, G. (1996). Visualization of gene expression in living adult *Drosophila*. *Science* **274**, 252–255.
35. Schubiger, M., and Palka, J. (1987). Changing spatial patterns of DNA replication in the developing wing of *Drosophila*. *Dev. Biol.* **123**, 145–153.
36. Gustafson, K., and Boulianne, G.L. (1996). Distinct expression patterns detected within individual tissues by the GAL4 enhancer trap technique. *Genome* **39**, 174–182.
37. Milán, M., Campuzano, S., and García-Bellido, A. (1997). Developmental parameters of cell death in the wing disc of *Drosophila*. *Proc. Natl. Acad. Sci. USA* **94**, 5691–5696.
38. Johnston, L.A., and Edgar, B.A. (1998). Wingless and Notch regulate cell-cycle arrest in the developing *Drosophila* wing. *Nature* **394**, 82–84.
39. Kiehart, D.P., Galbraith, C.G., Edwards, K.A., Rickoll, W.L., and Montague, R.A. (2000). Multiple forces contribute to cell sheet morphogenesis for dorsal closure in *Drosophila*. *J. Cell Biol.* **149**, 471–490.
40. Greco, V., Hannus, M., and Eaton, S. (2001). Argosomes: a potential vehicle for the spread of morphogens through epithelia. *Cell* **106**, 633–645.
41. Uehata, M., Ishizaki, T., Satoh, H., Ono, T., Kawahara, T., Morishita, T., Tamakawa, H., Yamagami, K., Inui, J., Maekawa, M., and Narumiya, S. (1997). Calcium sensitization of smooth muscle mediated by a Rho-associated protein kinase in hypertension. *Nature* **389**, 990–994.
42. Winter, C.G., Wang, B., Ballew, A., Royou, A., Kares, R., Axelrod, J.D., and Luo, L. (2001). *Drosophila* Rho-associated kinase (Drok) links Frizzled-mediated planar cell polarity signaling to the actin cytoskeleton. *Cell* **105**, 81–91.
43. Martín, F.A., Herrera, S.C., and Morata, G. (2009). Cell competition, growth and size control in the *Drosophila* wing imaginal disc. *Development* **136**, 3747–3756.
44. Mao, Y., Tournier, A.L., Bates, P.A., Gale, J.E., Tapon, N., and Thompson, B.J. (2011). Planar polarization of the atypical myosin Dachs orients cell divisions in *Drosophila*. *Genes Dev.* **25**, 131–136.
45. Irvine, K.D., and Wieschaus, E. (1994). fringe, a Boundary-specific signaling molecule, mediates interactions between dorsal and ventral cells during *Drosophila* wing development. *Cell* **79**, 595–606.